

Original Research

miR-215-5p Plays a Key Role in Suppressing Vascular Invasion and Recurrence in Hepatocellular Carcinoma by Blocking Vasculogenic Mimicry

Heng Zhang^{1,†}, Xi Lan^{2,†}, Liquan Cai¹, Xunfeng Gao¹, Feng Gao¹, Dan Yu¹, Jinlong Zhang¹,
Jinhui Zhang^{1,*} , Qinwen Tai^{1,*} ¹General Surgery Center, Shenzhen Hospital, Southern Medical University, 518000 Shenzhen, Guangdong, China²Clinical Laboratory Center, Shenzhen Hospital, Southern Medical University, 518000 Shenzhen, Guangdong, China*Correspondence: zhangjinhui2001@126.com (Jinhui Zhang); taiqinwen0302@163.com (Qinwen Tai)

†These authors contributed equally.

Academic Editor: Gary Hardiman

Submitted: 12 August 2023 Revised: 12 November 2023 Accepted: 27 December 2023 Published: 27 February 2024

Abstract

Background: This research explores the significance of miR-215-5p and vasculogenic mimicry (VM) in forecasting the prognosis for hepatocellular carcinoma (HCC). **Methods:** We analyzed HCC-associated miRNA expression profiles using data from The Cancer Genome Atlas (TCGA) and the Gene Expression Omnibus (GEO). Samples included tissue and blood from 80 early-stage HCC patients and serum from 120 healthy individuals. Reverse transcription-quantitative polymerase chain reaction (RT-qPCR) was employed to measure miR-215-5p and zinc finger E-box binding homeobox 2 (*ZEB2*) gene expressions. Hematoxylin and eosin (H&E) and CD34/Periodic Acid-Schiff (PAS) double staining assessed VM presence in HCC tissue sections. Bioinformatics tools predicted interactions between miR-215-5p and *ZEB2*, confirmed through luciferase reporter assays. We also examined the impact of miR-215-5p or *ZEB2* overexpression on HCC cell invasion, migration, and VM formation using scratch, Transwell invasion assays, and Matrigel 3D cultures. **Results:** Bioinformatics analysis indicated that miR-215-5p was under-expressed in HCC, particularly in cases with vascular invasion, which correlated with worse patient outcomes. In contrast, *ZEB2*, targeted by miR-215-5p, was overexpressed in HCC. RT-qPCR validated these expression patterns in HCC tissues. Among the HCC patients, 38 were VM positive and 42 VM negative. Logistic regression highlighted a negative correlation between miR-215-5p levels and VM positivity in HCC tissues and a positive correlation for *ZEB2* with VM positivity and tumor vascular invasion. Lower miR-215-5p levels were linked to increased HCC recurrence and metastasis. Both bioinformatics analysis and luciferase assays demonstrated a direct interaction between miR-215-5p and *ZEB2*. Enhancing miR-215-5p levels reduced *ZEB2* expression, consequently diminishing invasion, migration, and VM formation of the HCC cells *in vitro*. **Conclusions:** miR-215-5p expression inversely correlates with VM occurrence in HCC tissues, while *ZEB2* expression shows a direct correlation. By targeting *ZEB2*, miR-215-5p may hinder VM in HCC tissues, helping to prevent vascular invasion and HCC recurrence. Thus, miR-215-5p emerges as a vital prognostic indicator for predicting vascular invasion and recurrence in HCC.

Keywords: hepatocellular carcinoma; mir-215-5p; *ZEB2*; vasculogenic mimicry; vascular invasion; recurrent metastasis

1. Introduction

Hepatocellular carcinoma (HCC) is a highly aggressive liver cancer, and its severity is largely influenced by its capacity for vascular invasion and metastasis [1]. Vasculogenic mimicry (VM) is a distinct angiogenesis form characterized by tumor cells forming tubular structures that functionally resemble blood vessels, thereby aiding tumor growth and dispersal [2]. Recent evidence indicates that HCC tissues exhibit VM, while malignant cells imitate endothelial cells to form these structures, enabling nutrient supply and metastasis independently of the normal vascular network [3,4]. The presence of VM in HCC is strongly linked to the malignancy of the tumor, thus making inhibiting VM a key focus in HCC treatment strategies.

miRNAs, non-coding RNAs that regulate gene expression, are pivotal in the development and progression

of various malignancies [5]. Specifically, miR-215-5p, which binds to the 3' untranslated region (3' UTR) of its target genes, plays a significant role in various biological processes and diseases [6]. It modulates LPS-induced inflammation via the NF- κ B pathway [7] and is implicated in Alzheimer's disease by targeting brain-derived neurotrophic factor (BDNF), leading to neuronal apoptosis and cognitive decline [8]. Moreover, miR-215-5p is associated with diseases such as inflammatory bowel disease, pulmonary fibrosis, myocardial injury, and osteoporosis [9–12] and has been linked to the prognosis of cancers, including breast, prostate, lung, liposarcoma, and colorectal cancers [13–16]. In HCC, miR-215-5p is inversely related to VM and can inhibit vascular invasion and recurrent metastasis by targeting the zinc finger E-box binding homeobox 2 (*ZEB2*) gene, thus obstructing epithelial–mesenchymal transition (EMT) and VM formation in HCC cells [17–19].



Therefore, miR-215-5p could be a new biomarker for HCC diagnosis, treatment, and prognostic evaluation.

ZEB2 a gene encoding a transcription factor, plays a vital role in gene transcription regulation, affecting cell polarity, EMT, and tumor metastasis and invasion processes [20]. The *ZEB2* gene has been implicated in the progression and metastasis of various tumors, including esophageal, breast, lung, and ovarian cancers, with its high expression linked to increased tumor invasion and metastasis [21–25]. miR-215-5p can regulate *ZEB2* expression, influencing the development of both benign and malignant conditions [10,26,27]. However, the specific mechanism through which miR-215-5p regulates *ZEB2* in HCC growth and metastasis remains to be fully understood.

This study aimed to investigate the expressions of miR-215-5p and *ZEB2* in HCC tissues and their association with VM. By analyzing HCC-related miRNA expression profiles from The Cancer Genome Atlas (TCGA) and Gene Expression Omnibus (GEO) databases, we seek to evaluate the prognostic significance of miR-215-5p, *ZEB2*, and VM in HCC patients. This research will illuminate the role of miR-215-5p in HCC development and progression, its interplay with VM, and its potential use in HCC treatment. Our findings will offer novel insights and approaches for HCC therapy and contribute to the development of new markers for early prediction and clinical management of HCC.

2. Materials and Methods

2.1 GEO and TCGA Databases to Download HCC-Related Microarray Datasets for Target Gene Screening

We sourced HCC-related miRNA expression datasets (GSE6857, GSE36915, GSE67140) and a gene expression dataset (GSE33006) from the GEO database. GSE6857 comprised 241 tumor samples alongside paracancer normal controls; GSE36915 included 68 tumor samples and 21 non-tumor liver tissues; GSE67140 consisted of 91 HCC samples without vascular invasion and 81 with vascular invasion; GSE33006 encompassed 3 normal controls and 3 HCC samples. Additionally, HCC-related miRNA, gene expression profiles, and survival data were obtained from TCGA via the UCSC Xena platform (<https://xena.ucsc.edu/>), including data from 375 HCC and 50 normal tissues. For differential gene expression analysis in HCC, we utilized the “limma” package in R (Bioconductor, Buffalo, NY, USA), setting a significance threshold of $p < 0.05$ for filtering. Kaplan–Meier survival analysis was conducted using the “survival” package in R, with genes exhibiting a p -value of less than 0.05 deemed prognostically significant. To identify potential miRNA target genes, we accessed databases including miRDB (<http://mirdb.org/>), miRDIP (<http://ophid.utoronto.ca/mirDIP/>), RNAInter (<http://www.rnainter.org/>), and miRmap (<https://mirmap.ezlab.org/>).

2.2 Clinical Sample Collection

Our study focused on 80 early-stage HCC patients who underwent comprehensive HCC surgery at Shenzhen Hospital, Southern Medical University, from December 2017 to December 2022 (HCC group). The postoperative pathological staging adhered to the criteria set by the Korean HCC Study Group (KLCSG) and the National Cancer Center (NCI) [28].

The inclusion criteria were (1) patients who had undergone radical HCC surgery at Shenzhen Hospital, Southern Medical University, with post-surgical pathological confirmation of HCC; (2) no preoperative anti-cancer treatments such as immunotherapy; (3) complete medical documentation for each patient; (4) no significant diseases or dysfunctions in major organs, and normal results in routine blood, urine, feces, liver function, kidney function, and cardiac function tests.

The exclusion criteria included: (1) Patients with non-alcoholic fatty liver-related HCC; (2) patients with secondary HCC; (3) individuals with other malignant tumors; (4) patients who had received radiotherapy prior to their radical HCC surgery; (5) patients recently treated with molecularly targeted therapies.

The preoperative Barcelona Clinic Liver Cancer (BCLC) staging for the patients is detailed in **Supplementary Table 1**. Patient follow-ups commenced in January 2022. Additionally, serum samples from 120 healthy individuals, randomly selected from those who underwent health check-ups at Shenzhen Hospital, Southern Medical University in the same period and showed normal results, were used as control samples. HCC tissues and corresponding paracancerous tissue wax blocks from enrolled patients were preserved for future analysis. All participants provided written informed consent, and the study protocol was approved by the Ethics Committee of Shenzhen Hospital, Southern Medical University.

2.3 Serum Sample Collection and Preservation

In our study, venous blood was collected from the HCC and the control groups. Following collection, the blood samples were allowed to clot naturally at 37 °C, then refrigerated at 4 °C overnight to ensure proper clot formation. Subsequently, the samples were centrifuged at 3000 rpm for 10 minutes at 4 °C to separate the serum, discarding any insoluble material. Then, the clear serum was carefully transferred to sterile tubes, aliquoted into smaller volumes, and stored in an ultra-low temperature freezer for future use. During the entire process of serum collection and storage, efforts were made to minimize the exposure time of the specimens to ambient conditions to prevent RNA degradation, which could potentially impact the accuracy of the experimental results.

2.4 Reverse Transcription-Quantitative Polymerase Chain Reaction (RT-qPCR)

For RNA extraction, 200 μL of serum previously stored in ultra-low temperature conditions was processed using the miRNeasy Mini Kit (217084, Qiagen, Germany). We diluted 5 μL of the RNA sample 20 times in RNase-free water (N003-1-1, Beijing Lingbao Technology Co., Ltd., Beijing, China) and measured its absorbance at 260 nm and 280 nm using a UV spectrophotometer. This step was crucial to ascertain the concentration and purity of the RNA. We considered samples with an $\text{OD}_{260}/\text{OD}_{280}$ ratio ranging from 1.7 to 2.1 to be high in purity and suitable for further analysis.

PolyA-tailed cDNA was synthesized using the PolyA Tailing Assay Kit (B532451, Sangon, Shanghai, China) in a PCR thermocycler (Applied Biosystems, Foster City, CA, USA). This process involved the addition of reverse transcription reaction components and a set of universal PCR primers (R), resulting in cDNA that included miRNAs with a polyA tail.

We conducted real-time PCR using the ABI 7500 Real-time PCR System (Applied Biosystems, USA). The 20 μL PCR mixture contained 10 μL of $2\times$ real-time PCR buffer (A44941, Invitrogen, Foster City, CA, USA), 0.32 μL of specific primer pairs (5 mmol/ μL), 0.2 μL of Taq DNA polymerase (5×10^6 U/L), 2 μL of cDNA template, and sufficient RNase-free water to bring the final volume up to 20 μL . The PCR cycling conditions included an initial denaturation at 95 $^{\circ}\text{C}$ for 3 minutes, followed by cycles of denaturation at 94 $^{\circ}\text{C}$ for 30 seconds, annealing at 55 $^{\circ}\text{C}$ for 30 seconds, and extension at 72 $^{\circ}\text{C}$ for 30 seconds, for a total of 30 cycles. Each sample was tested in triplicate. The Ct value (threshold cycle) was determined by selecting the threshold value at the lowest point of the parallel rise in the logarithmic amplification curve. Data analysis was performed using the $2^{-\Delta\Delta\text{Ct}}$ method, and details of the primer sequences are provided in **Supplementary Table 2**.

2.5 Hematoxylin and Eosin (H&E) Staining

We prepared tissue sections from wax-embedded HCC and adjacent normal tissues using a microtome. These sections were carefully floated on warm water before being mounted onto slides and dried in preparation for staining. The staining process began with dewaxing the sections, followed by staining with hematoxylin. Then, we differentiated the sections using hydrochloric acid ethanol and dehydrated them through a series of graded ethanol solutions before, finally, mounting them using neutral gum. Thereafter, these prepared slides were ready for examination under a light microscope (globalspec, Waltham, MA, USA).

2.6 CD34/Periodic Acid-Schiff (PAS) Double Staining

Initially, CD34 immunohistochemical staining was applied to the tissue sections. Subsequently, these sections underwent a series of treatments: Immersion in distilled wa-

ter for 2–3 minutes, a 10-minute periodate solution soak, and a rinse in distilled water. This was succeeded by PAS staining for 20 minutes, another rinse, and then a 1-minute hematoxylin application for light nuclear staining. After a brief rinse in distilled water, we used hydrochloric acid ethanol for differentiation. Next, the sections were subjected to the same series of steps as H&E staining: Bluing, dehydration, clearing, and mounting. The final step involved observing the stained slides under a light microscope to identify CD34 and PAS signals and count the formation of tube-like structures, as referenced in [29].

2.7 Determination of Staining Results

H&E stained sections were first observed microscopically to determine VM roughly. VM was surrounded by tumor cells without hemorrhage, necrosis, or inflammatory cell infiltration. The luminal structure of CD34-positive ducts showed endothelium-dependent vasculature. VM was surrounded by plasticized tumor cells rather than endothelial cells and lined with PAS-positive rings. Erythrocytes may or may not be present in the lumen. Determination of endothelium-dependent vessels included looking for PAS-stained vessels under $100\times$ light microscopy. CD34-positive microscopy showed brownish-yellow granular staining of the vascular endothelial cell cytosol. The microvessels were counted in a microscopic $100\times$ field of view, which covered the entire tissue. The area of concentrated endothelium-dependent vessels was selected randomly, and the sum of vessels in three high-magnification fields was counted as the microvascular density (MVD). Microvessels comprised single or clusters of brown CD34-positive endothelial cells [30].

2.8 Immunohistochemistry (IHC)

In our study, IHC was performed on a set of 80 HCC samples. For this, we used anti-ZEB2 antibodies (Solarbio, K106922P, 1:100, Beijing, China) in accordance with a standardized staining protocol. To quantitatively analyze the protein expression indicated by the IHC staining, we utilized an Olympus BX51 image analysis system, complemented by Olympus cellSens Dimension 1.5 Imaging software (Olympus, Tokyo, Japan). Each stained section was scrutinized at a $200\times$ magnification, and from each sample, 10 representative fields of view were carefully selected and analyzed.

2.9 Dual-Luciferase Reporter Gene Assay

To predict potential complementary binding sites between miR-215-5p and the 3'UTR in the ZEB2 gene, we employed the TargetScan online software (https://www.targetscan.org/vert_40/). Then, we designed mutagenic primers for the potential binding site of miR-215-5p using a targeted mutation kit. The construction of vectors involved treating pGEMT-ZEB2 3'UTR-WT and pGEMT-ZEB2 3'UTR-MUT, along with the pmirGLO vector, with restriction en-

donucleases Pme I and Sal I in a water bath at 37 °C overnight. Post-digestion, the products underwent purification via agarose gel electrophoresis and gel extraction. The purified pmir-GLO vector was then ligated with the ZEB2 3'UTR-WT/MUT fragment in the presence of T4 DNA ligase at 4 °C overnight. These steps led to the amplification of the wild-type and mutant recombinant pmir-GLO vectors, named ZEB2-WT and ZEB2-MUT, respectively. PCR amplification was performed on a small volume of the amplified bacterial broth, followed by identification through 1.5% agarose gel electrophoresis. Positive clones of the recombinant plasmids were selected and subsequently sent to Nanjing Kingsray Biotechnology Co.

For the cellular assays, HEK293T cells (Item No. ACS-4500, ATCC, MA, USA) were seeded in 24-well plates and cultured in DMEM (Gibco, USA) supplemented with 10% fetal bovine serum (16140089, Gibco, USA), 10 µg/mL streptomycin, and 100 U/mL penicillin. All cell lines were validated by STR profiling and tested negative for mycoplasma. The cells were incubated overnight at 37 °C with 5% CO₂ in a humidity-controlled incubator. At 70% confluency, the cells were transfected with either miR-215-5p mimics or Negative Control (NC) miR-215-5p along with the recombinant pmirGLO vector (pmirGLO ZEB2 3'UTR-WT or pmirGLO-ZEB2 3'UTR-MUT), using Lipofectamine 2000 transfection reagent (11668019, Invitrogen, USA). After 48 hours post-transfection, the cells were lysed and centrifuged at 12,000 g for 1 minute, and the supernatant was collected for analysis. The Dual-Luciferase Reporter Assay System (E1910, Promega, Beijing, China) was utilized to detect luciferase activity. In each assay, 100 µL of firefly luciferase working solution and sea kidney luciferase working solution were added consecutively to measure firefly and Renilla luciferase activities, respectively. The results are expressed as the ratio of firefly luciferase to Renilla luciferase activity.

2.10 Cell Culture and Transfection

We acquired HCC cell lines HCCLM3, Huh-7, MHCC97L, and Hep G2, as well as the normal hepatocyte THLE-2 cell line from ATCC, USA. All cell lines were validated by STR profiling and tested negative for mycoplasma. Cells were all cultured in a humidified incubator at 37 °C and 5% CO₂. The HCC cell lines (HCCLM3, Huh-7, MHCC97L, Hep G2) were maintained in DMEM (11960044, Gibco, USA) enriched with 10% fetal bovine serum (Gibco, USA), 100 µg/mL streptomycin, and 2100 U/mL penicillin. The normal hepatocyte line THLE-2 was cultured in RPMI-1640 (11875101, Gibco, USA) supplemented with 10% fetal bovine serum (51023126, Gibco, USA), 100 µg/mL streptomycin, and 100 U/mL penicillin. Cells in the logarithmic growth phase were trypsinized and seeded in 6-well plates at a density of 1×10^5 cells per well for 24 hours. Upon reaching about 75% confluency, the

cells underwent transient transfection, following the protocol provided alongside the Lipofectamine 2000 reagent (Invitrogen).

The experimental groups included the NC mimic group, miR-215-5p mimic group, oe-NC group (overexpression of null control plasmid), oe-ZEB2 group (overexpression of ZEB2 plasmid), and the miR-215-5p mimic + ZEB2 group. Transfection plasmids and mimics were sourced from Sino Biological (Beijing, China). Post-transfection (after 6 hours), the medium was changed, and cells were cultured for an additional 48 hours before collection for downstream analyses. The relevant gene expressions in each group were assessed 48 hours post-transfection using qPCR and Western blot techniques, as detailed in references [31,32].

2.11 Western Blot

Protein extraction from the cultured cells was performed for subsequent electrophoresis and Western blotting analysis. The protein concentrations were determined using a Bicinchoninic Acid (BCA) Protein Assay Kit (20201ES76, Yisheng Biotechnology Co., Ltd., Shanghai, China). The proteins were then separated by standard Sodium Dodecyl Sulfate-Polyacrylamide Gel Electrophoresis (SDS-PAGE) and transferred onto Polyvinylidene Difluoride (PVDF) membranes. These membranes were blocked at room temperature using 5% Bovine Serum Albumin (BSA) for 1 hour. Subsequently, we added the primary antibodies, ZEB2 (ab214425, 1:1000, Abcam, Cambridge, UK) and Glyceraldehyde 3-phosphate dehydrogenase (GAPDH) (ab8245, 1:5000, Abcam, UK) and incubated the membranes overnight at 4 °C with gentle shaking. Post-incubation, the membranes were washed three times with Tris-buffered saline with 0.1% Tween® 20 Detergent (TBS-T), each for 5 minutes. Detection was carried out using an enhanced chemiluminescence assay following another three 5-minute TBS-T washes. For protein quantification, we used ImageJ 1.48v software (National Institutes of Health, Bethesda, MD, USA), employing the ratio of the gray value for each protein to that of the GAPDH internal reference protein.

2.12 Cell Scratch Assay

The plasmids were left to transfect for 48 h before the fused cells were scraped off using a sterile 200 µL pipette tip. Separated cells and debris were removed by PBS washing. The scratch distance was photographed microscopically and set as 0 h. After incubation in a serum-free DMEM medium for 48 h, the same observation position was taken. The scratch distance was photographed again and compared with the 0 h cell scratch distance to observe the migration distance.

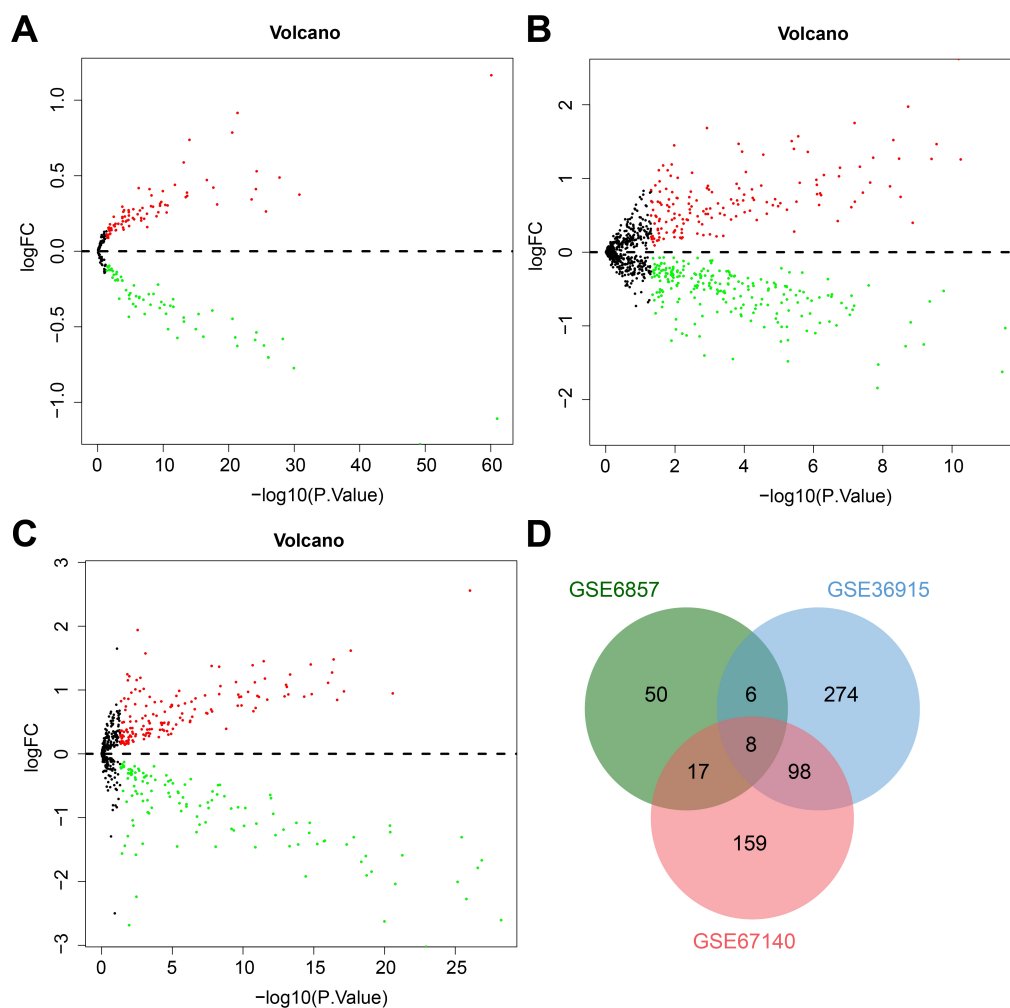


Fig. 1. Bioinformatics analysis to screen miRNAs associated with vascular invasion in hepatocellular carcinoma (HCC). Note: (A) Volcano plot of differentially expressed miRNAs between HCC samples ($n = 241$) and normal liver tissue samples ($n = 241$) in GSE6857. (B) Volcano plot of differentially expressed miRNAs between HCC samples ($n = 68$) and normal liver tissue samples ($n = 21$) in GSE36915. (C) Volcano plot of differentially expressed miRNAs between HCC samples without vascular invasion ($n = 91$) and HCC samples with vascular invasion ($n = 81$) in GSE67140. Red dots indicate high expression, and green dots indicate low expression. (D) Overlapping differentially expressed miRNAs in the three datasets.

2.13 Transwell Assay

For the invasion assay, we coated the upper surface of the Transwell membranes with BD Matrigel (356234, Bedford, MA, USA) and allowed it to gel at 37°C for 30 minutes. Prior to use, the basement membrane was hydrated. Cells were serum-starved for 12 hours to facilitate the assay. Afterward, these cells were collected and resuspended in a serum-free medium at a concentration of 1×10^5 cells/mL. The lower chamber of the Transwell apparatus was filled with a medium containing 10% fetal bovine serum. We then added $100 \mu\text{L}$ of the cell suspension to the upper chamber.

Following a 24-hour incubation at 37°C , cells that did not invade through the Matrigel membrane were carefully removed with cotton swabs. The cells that penetrated the membrane were fixed with 100% methanol and stained with 1% toluidine blue (89640, Sigma, Kawasaki, Japan). We

then counted the stained, invading cells under an inverted light microscope, selecting five random fields for analysis, as detailed in reference [33].

2.14 Three-Dimensional Cultures

Post-transfection (24 hours), tumor cells were incorporated into a Matrigel matrix (356234, Bedford, MA, USA) to induce polymerization. During a 10-day incubation period in the 3D culture, we employed both pretreatment and continuous treatment protocols using conditioned media supplemented with 10% fetal bovine serum (Hyclone). For RNA and protein extraction, cells embedded in Matrigel were retrieved using trypsin digestion. Following this, we used Trizol and RIPA buffer to isolate total RNA and protein from the cells, respectively, as outlined in reference [34].

2.15 Statistical Methods

For our data analysis, we utilized SPSS statistical software. Quantitative data were presented as mean \pm standard deviation, and differences between the two groups were assessed using the independent samples *t*-test. Qualitative data, expressed in percentages or rates, were analyzed using the chi-square test. We employed two-way stepwise regression and the Akaike information criterion (AIC) for variable selection. Logistic regression models were used to investigate the association between VM expression and the risk of vascular invasion and recurrent metastasis in HCC tissues [4]. Additionally, the predictive accuracy of these models was evaluated using receiver operating characteristic (ROC) curves.

3. Results

3.1 Bioinformatics Exploration Reveals Eight miRNAs Linked to Vascular Invasion in HCC

To identify miRNAs potentially linked to vascular invasion in HCC, we analyzed miRNA expression data from the GEO database, specifically datasets GSE6857 and GSE36915. In the GSE6857 dataset, we found 81 miRNAs exhibiting differential expression in HCC cases, with 49 miRNAs being upregulated and 32 downregulated (as shown in Fig. 1A and detailed in **Supplementary Table 3**). Similarly, analysis of the GSE36915 dataset revealed 386 differentially expressed miRNAs in HCC, comprising 160 upregulated and 226 downregulated miRNAs (Fig. 1B, **Supplementary Table 4**).

Further analysis was conducted on the HCC vascular invasion-associated miRNA dataset, GSE67140. This revealed that, in HCC samples exhibiting vascular invasion, 156 miRNAs were upregulated, while 126 miRNAs were downregulated compared to HCC samples without vascular invasion (Fig. 1C, **Supplementary Table 5**). By intersecting data from these three datasets, we identified eight potential candidate miRNAs: hsa-miR-335, hsa-miR-340, hsa-miR-215-5p, hsa-let-7c, hsa-miR-203, hsa-miR-214, hsa-miR-224, and hsa-miR-181c (Fig. 1D, **Supplementary Table 6**).

3.2 Low miR-215-5p Expression is Associated with Poor Prognosis in HCC Patients and may be Involved in Vascular Invasion in HCC

In our quest to pinpoint miRNAs that can predict patient outcomes for HCC, we investigated the link between the eight identified miRNAs and overall patient survival, utilizing data from the TCGA database. Kaplan–Meier survival analysis revealed a notable correlation: HCC patients with elevated levels of hsa-miR-215-5p demonstrated significantly improved overall survival compared to those with lower expression levels. In contrast, the remaining seven miRNAs (hsa-miR-335, hsa-miR-340, hsa-let-7c, hsa-miR-203, hsa-miR-214, hsa-miR-224, and hsa-miR-

181c) showed no substantial impact on the overall survival of HCC patients (as depicted in Fig. 2). Consequently, miR-215-5p was chosen for further investigation.

Furthermore, as depicted in Fig. 3, miR-215-5p was markedly downregulated in HCC tissues compared to normal tissues in TCGA, GSE6857, and GSE36915 datasets. Specifically, in the GSE67140 dataset, miR-215-5p expression was significantly lower in HCC samples with vascular invasion than in those without vascular invasion.

3.3 miR-215-5p may Affect HCC Vascular Invasion by Targeting ZEB2

To elucidate the mechanism through which miR-215-5p regulates vascular invasion in HCC, we utilized a range of bioinformatics resources, including miRDB, mirDIP, RNAInter, and miRmap, to predict the miR-215-5p target genes. Our analysis identified six potential target genes that were common across these databases (as shown in Fig. 4A and listed in **Supplementary Table 7**). Additionally, we conducted a differential gene expression analysis on the GSE33006 dataset with the criteria of $|\log_{2}FC| > 1$ and $p < 0.05$. This analysis revealed 2806 genes with differential expressions in HCC, including 1526 genes that were upregulated (Fig. 4B, **Supplementary Table 8**). By intersecting these upregulated genes with the predicted targets of miR-215-5p, we pinpointed *ZEB2* as a gene of interest (Fig. 4C). *ZEB2* a factor known for regulating EMT, plays a crucial role in tumor invasion and metastasis. Moreover, existing studies suggest that *ZEB2* could be instrumental in promoting angiogenesis in HCC [35]. Therefore, we hypothesize that miR-215-5p may affect vascular invasion in HCC by targeting *ZEB2*.

3.4 miR-215-5p is Lowly Expressed in HCC Patients, and ZEB2 is Highly Expressed

Our study revealed no significant differences in gender, age, smoking habits, or alcohol consumption between the HCC group and the control group, with all *p*-values exceeding 0.05. To assess the expression levels of miR-215-5p and *ZEB2*, PCR analysis was conducted on serum samples from both HCC patients and healthy individuals. The results indicated a notable downregulation of miR-215-5p and an upregulation of *ZEB2* in the serum of HCC patients compared to the control group. The variations in the expression levels of both miR-215-5p and *ZEB2* were statistically significant, with all *p*-values falling below 0.05, as detailed in **Supplementary Table 9**.

3.5 miR-215-5p Targets ZEB2 in HCC and is Associated with VM

H&E staining revealed distinct cellular changes in HCC tissues compared to adjacent normal liver tissue. Notably, HCC cells were polygonal, densely packed, and disorganized, disrupting the hepatic lobular structure. Infiltration of inflammatory cells and tumor cells forming tubu-

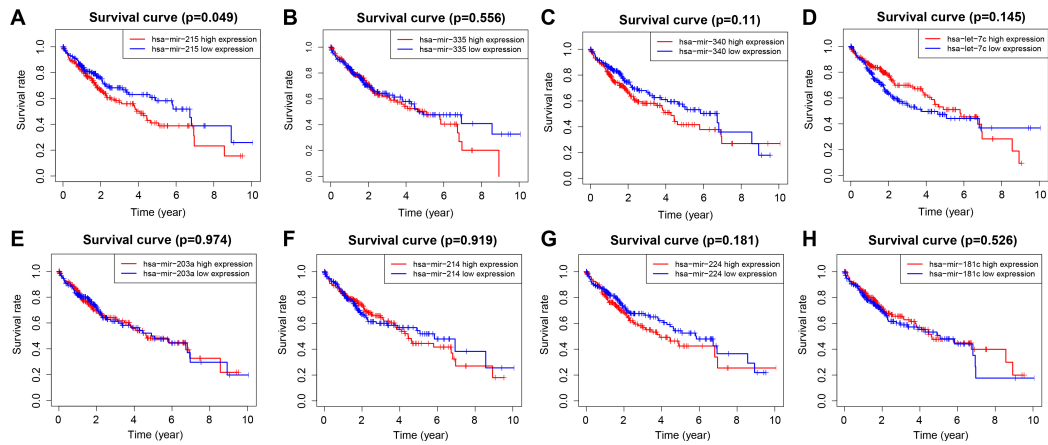


Fig. 2. Kaplan–Meier curve analysis of the correlation between eight miRNAs and the overall survival prognosis of HCC patients. Note: analysis of hsa-miR-215-5p (A), hsa-miR-335 (B), hsa-miR-340 (C), hsa-let-7c (D), hsa-miR-203 (E), hsa-miR-214 (F), hsa-miR-224 (G) and hsa-miR-181c (H) correlated with the overall survival prognosis of HCC patients.

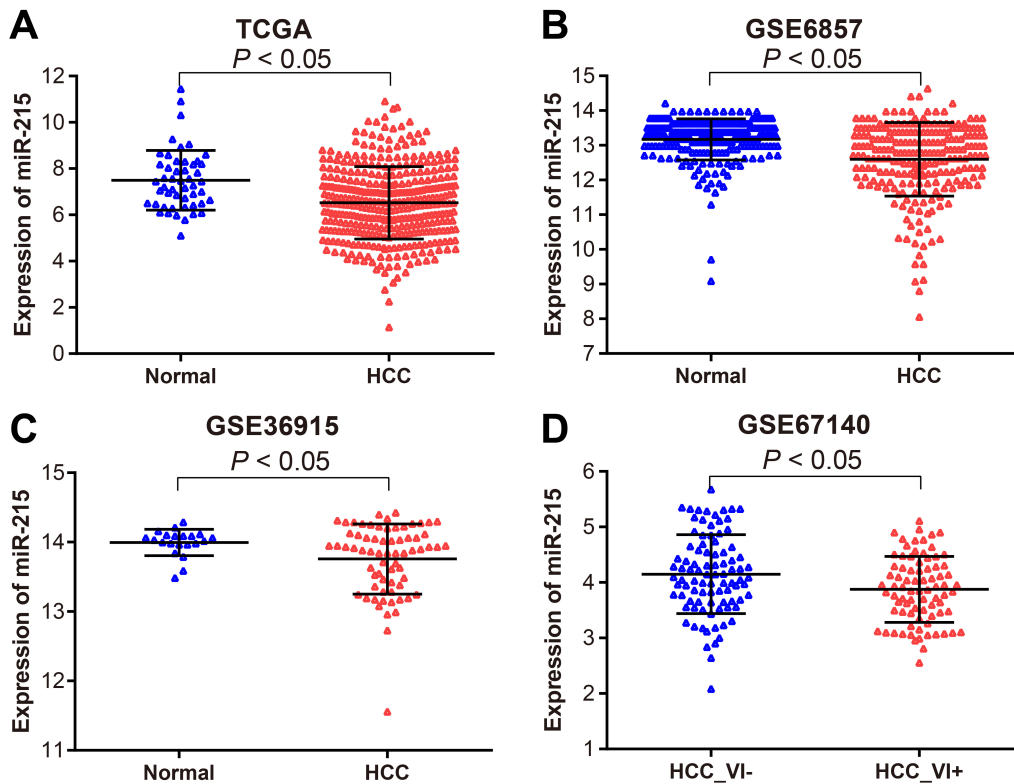


Fig. 3. miR-215-5p expression in HCC-related datasets in The Cancer Genome Atlas (TCGA) and Gene Expression Omnibus (GEO) databases. Note: expression levels of miR-215-5p in TCGA datasets (A), GSE6857 (B), GSE36915 (C), and GSE67140 (D). vi, vascular invasion.

lar structures containing erythrocytes were also observed (Fig. 5A). Moreover, CD34/PAS double staining indicated VM presence in 38 (47.5%) out of 80 HCC samples, while 42 samples were VM negative (Fig. 5B). A significant increase in VM formation was noted in VM-positive tissues compared to VM-negative ones.

RT-PCR assays demonstrated that miR-215-5p expression was significantly lower in both VM-positive and

VM-negative HCC samples than in normal tissue, with the levels even lower in VM-positive samples. Conversely, *ZEB2* expression levels were elevated in both VM groups, particularly in VM-positive samples (all $p < 0.05$, Fig. 5C). Western blot and immunohistochemistry (IHC) results further confirmed that *ZEB2* expression was significantly higher in HCC tissues, especially in the VM-positive group (Fig. 5D,E).

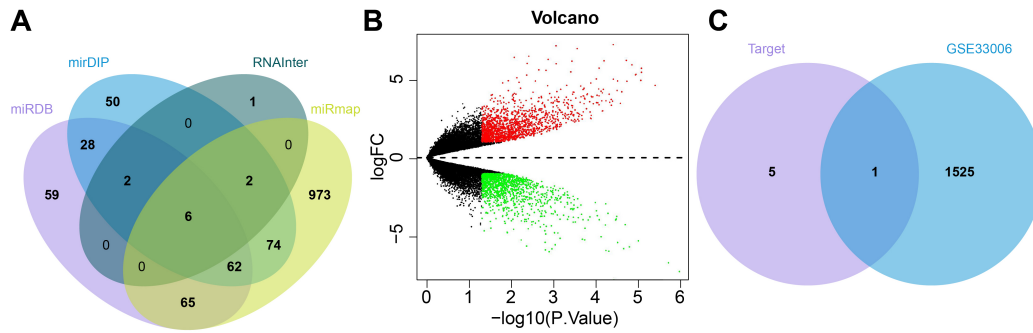


Fig. 4. Prediction of miR-215-5p target genes in HCC. Note: (A) The miRDB, mirDIP, RNAInter, and miRmap databases were used to predict the miR-215-5p target genes. (B) The Volcano plot shows the differentially expressed genes between HCC and normal samples in GSE33006. (C) The overlap between the miR-215-5p target genes and the upregulated genes in HCC.

To explore the interaction between miR-215-5p and *ZEB2*, the TargetScan database was used to identify the potential binding site between them (Fig. 5F). Dual-luciferase reporter assays indicated a significant reduction in luciferase activity of *ZEB2*-WT with miR-215-5p overexpression, whereas the mutant group showed no change. This suggests a direct interaction between miR-215-5p and *ZEB2* (Fig. 5G).

3.6 VM Positive Expression Rate in HCC Tissues is Closely Associated with Vascular Invasion and Recurrent Metastasis

Research has demonstrated that MVD is a primary indicator of tumor neovascularization, while VM significantly contributes to tumor blood supply [36]. VM is closely related to higher tumor grade and stage, and MVD is associated with increased tumor size, grade, and stage [37]. Moreover, a notable link exists between tumor cell proliferation, VM formation, and MVD [38].

In our study, as detailed in **Supplementary Table 10**, notable differences were observed between VM-positive and VM-negative HCC groups in terms of tumor size, differentiation, Tumor, Node, Metastasis (TNM) stage, cirrhosis level, MVD, preoperative Alpha-Fetoprotein (AFP), BCLC stage, and expressions of miR-215-5p and *ZEB2* (all $p < 0.05$). VM positivity was significantly associated with vascular invasion and recurrent metastasis in HCC (all $p < 0.05$).

Logistic regression analysis evaluated the relationship between VM expression, vascular invasion, and recurrent metastasis as dependent variables, and factors, such as age, gender, smoking and drinking history, miR-215-5p and *ZEB2* expressions, tumor size, differentiation, TNM stage, cirrhosis, MVD, and preoperative AFP levels as independent variables.

In analyzing the VM-positive rate, miR-215-5p expression, *ZEB2* expression, and tumor size were significant ($p < 0.05$). Specifically, miR-215-5p expression was inversely correlated with VM positivity, while *ZEB2* expression showed a positive correlation (**Supplementary Ta-**

ble 11). In assessing factors linked to vascular invasion in HCC, *ZEB2* expression and tumor size were significant ($p < 0.05$), with a notable positive correlation found for *ZEB2* expression (**Supplementary Table 12**). For factors associated with recurrence and metastasis in HCC, significant variables included miR-215-5p expression, tumor size, and preoperative AFP levels ($p < 0.05$), with miR-215-5p expression negatively correlated with recurrent metastasis (**Supplementary Table 13**).

ROC curve analysis was conducted for two final models to predict the likelihood of vascular invasion and recurrent metastasis. As illustrated in Fig. 6A and **Supplementary Table 14**, the model predicting vascular invasion, which included gender and *ZEB2* expression, showed an area under the curve (AUC) of 0.940 (95% CI: 0.886–0.993) for tumor size and 0.900 (95% CI: 0.824–0.977) for TNM stage. The AUC for the model incorporating all predictor variables was 0.959 (95% CI: 0.915–1.000).

In the model predicting recurrent metastasis, including alcohol consumption history, miR-215-5p expression, *ZEB2* expression, and TNM stage (Fig. 6B and **Supplementary Table 15**), the AUC was 0.941 (95% CI: 0.889–0.994) for tumor size, 0.888 (95% CI: 0.807–0.968) for cirrhosis, and 0.772 (95% CI: 0.664–0.881) for preoperative AFP. The AUC for the model with all predictor variables was 0.965 (95% CI: 0.930–1.000). These results underscore the strong association between VM positivity and the incidence of vascular invasion and recurrent metastasis in HCC.

3.7 Upregulation of miR-215-5p Inhibits *ZEB2*, Leading to Reduced Invasion, Migration, and VM Formation in HCC Cells In Vitro

Several studies have indicated that the formation of VM in tumor cells mirrors the migration and invasion processes of endothelial cells [35,39,40]. To explore the impact of miR-215-5p on the invasive and proliferative capabilities of HCC cells, we first employed RT-PCR to assess the expression levels of miR-215-5p and *ZEB2* in the normal hepatocyte line THLE-2 and four HCC cell lines

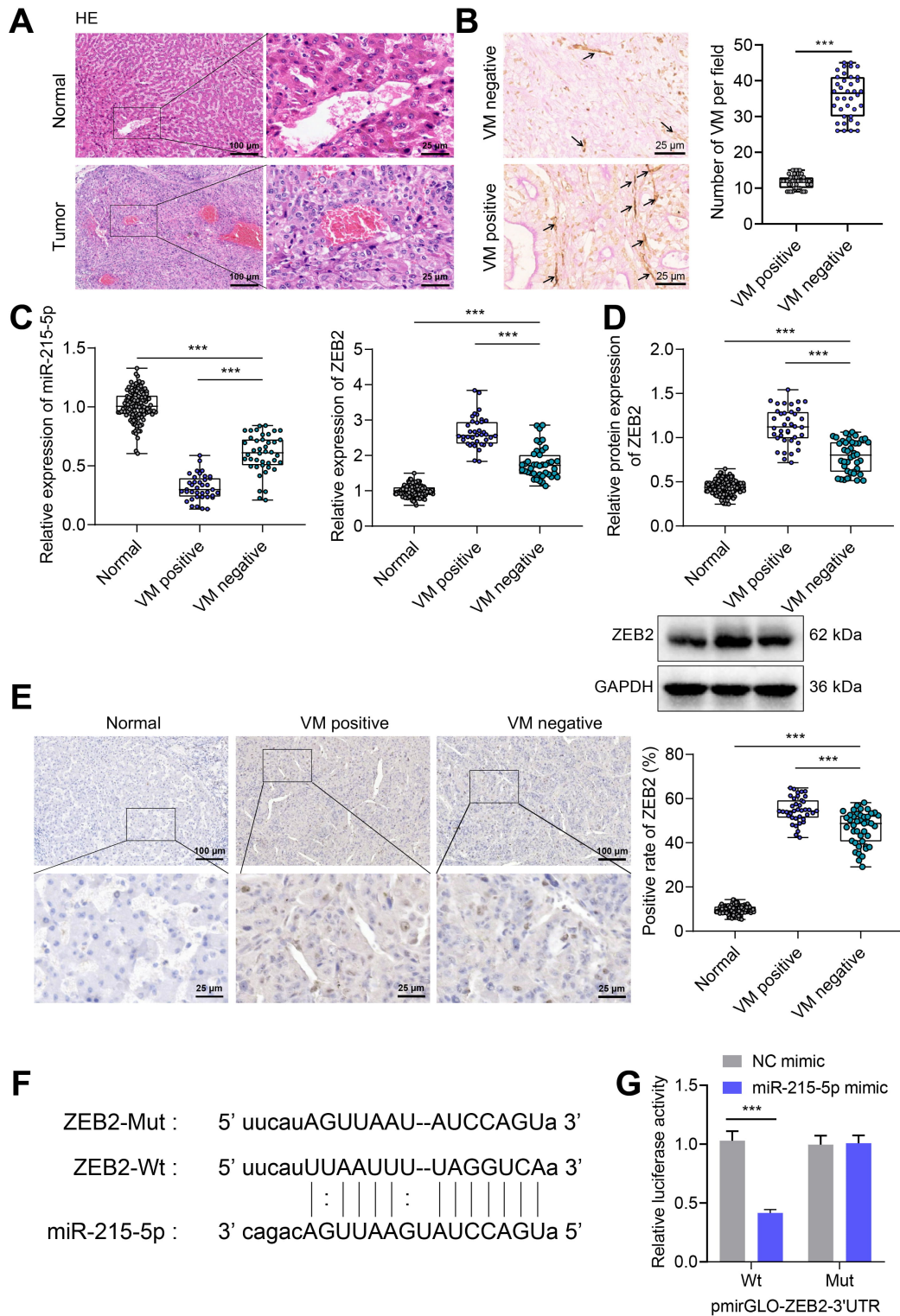


Fig. 5. Validation of miR-215-5p targeting relationship with zinc finger E-box binding homeobox 2 (*ZEB2*) in HCC and its correlation with vasculogenic mimicry (VM) expression. Note: (A) Hematoxylin and eosin (H&E) staining map of HCC tissues and normal tissues next to cancer ($\times 200$). (B) CD34/PAS double staining and quantification of VM in HCC tissues—black arrows indicate CD34 (+) and red arrows PAS (+). (C) RT-PCR detection of miR-215-5p and *ZEB2* in different tissues expression level changes in different tissues. (D) Western blot detection of *ZEB2* protein expression level changes in different tissues. (E) Immunohistochemistry (IHC) to detect *ZEB2* positive expression levels in different tissues. (F) RNA22 to predict the binding site of *ZEB2* and miR-215-5p. (G) Dual luciferase reporter assay to detect whether miR-215-5p could bind *ZEB2*, In the connected group data, *** indicates $p < 0.001$. GAPDH, Glyceraldehyde 3-Phosphate Dehydrogenase.

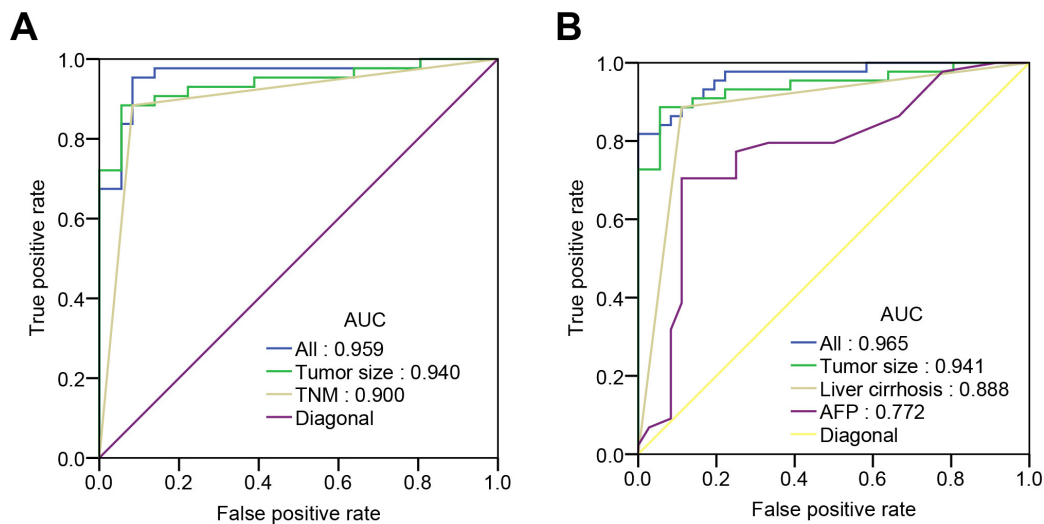


Fig. 6. Predictive accuracy of receiver operating characteristic (ROC) curve evaluation model for HCC vascular invasion (A) and recurrent metastasis (B). Note: In the figure, “tumor size” indicates the model that includes tumor size, “TNM” indicates the model that includes the TNM stage, and “all” indicates the model that includes all predictive variables at the same time. The horizontal coordinates are the false positive rate, and the vertical coordinates are the true positive rate. In the area under the curve (AUC) comparison by the Delong test.

(HCCLM3, Huh-7, MHCC97L, and Hep G2). Our findings revealed a significant reduction in miR-215-5p and an increase in *ZEB2* expression across all HCC cell lines compared to THLE-2, with Hep G2 showing the most pronounced changes; thus, it formed the primary focus for further functional assays (Fig. 7A).

Subsequently, Hep G2 cells were transfected with different plasmids, resulting in groups: NC mimic, miR-215-5p mimic, oe-NC, oe-*ZEB2*, and miR-215-5p mimic+oe-*ZEB2*. Post-transfection, RT-PCR analysis of miR-215-5p and *ZEB2* expression (Fig. 7B) indicated a significant increase in miR-215-5p and a decrease in *ZEB2* expression in the miR-215-5p-mimic group compared to Negative Control (NC) mimic; in the oe-*ZEB2* group, *ZEB2* expression was significantly higher than in the oe-NC group. The miR-215-5p mimic+oe-*ZEB2* group showed a marked increase in miR-215-5p and a decrease in *ZEB2* expression compared to the oe-*ZEB2* group. Western blot analysis of *ZEB2* protein levels corroborated these PCR findings (Fig. 7C), confirming successful plasmid transfection.

We employed scratch and Transwell invasion assays to evaluate cell migration and invasion, respectively (Fig. 7D,E). Compared to the NC mimic group, the miR-215-5p mimic cells exhibited significantly reduced migration and invasion capabilities; the oe-*ZEB2* group showed enhanced migration and invasion compared to the oe-NC group; the miR-215-5p mimic+oe-*ZEB2* group displayed reduced migration and invasion compared to the oe-*ZEB2* group.

Additionally, we utilized a Matrigel 3D culture, a standard *in vitro* model, to assess VM formation (Fig. 7F). The results demonstrated that HepG2 cells in the miR-215-5p

upregulated group did not form typical tubular structures on the 3D Matrigel, whereas cells with upregulated *ZEB2* did. In cells with simultaneous overexpression of miR-215-5p and *ZEB2*, the ability to form tubular structures was diminished. These findings suggest that overexpression of miR-215-5p inhibits *ZEB2*, subsequently reducing the capacity of HCC cells to invade, migrate, and form VMs.

4. Discussion

Our research analyzed HCC-related miRNA expression datasets (GSE6857, GSE36915, and GSE67140) from the GEO database, identifying eight miRNAs linked to vascular invasion in HCC: hsa-miR-335, hsa-miR-340, hsa-miR-215-5p, hsa-let-7c, hsa-miR-203, hsa-miR-214, hsa-miR-224, and hsa-miR-181c. Prior studies have established that hsa-miR-335 suppresses HCC cell proliferation, migration, and invasion by targeting *BCL2L2*, *SOX4*, and *TNC*, respectively, with its downregulation correlating with HCC malignancy and poor prognosis [41]. hsa-miR-340, found to be downregulated in HCC, inhibits tumor growth and metastasis by affecting genes such as *JAK1* and *DCR3* [42, 43]. hsa-let-7c, broadly present in human tissues, is downregulated in HCC and inhibits tumor growth and metastasis by targeting *HMGA2* and *cyclin D1* [44]. hsa-miR-203, with reduced expression in various cancers, targets *ZEB1* and *HOXD3* to inhibit HCC growth and metastasis [45–47]. In contrast, hsa-miR-214, upregulated in multiple cancers, promotes HCC growth and metastasis by targeting *EZH2* [48]. Similarly, hsa-miR-224, upregulated in several cancers, enhances HCC growth and metastasis by affecting *AKT* and *HOXD10* [49]. hsa-miR-181c, which is

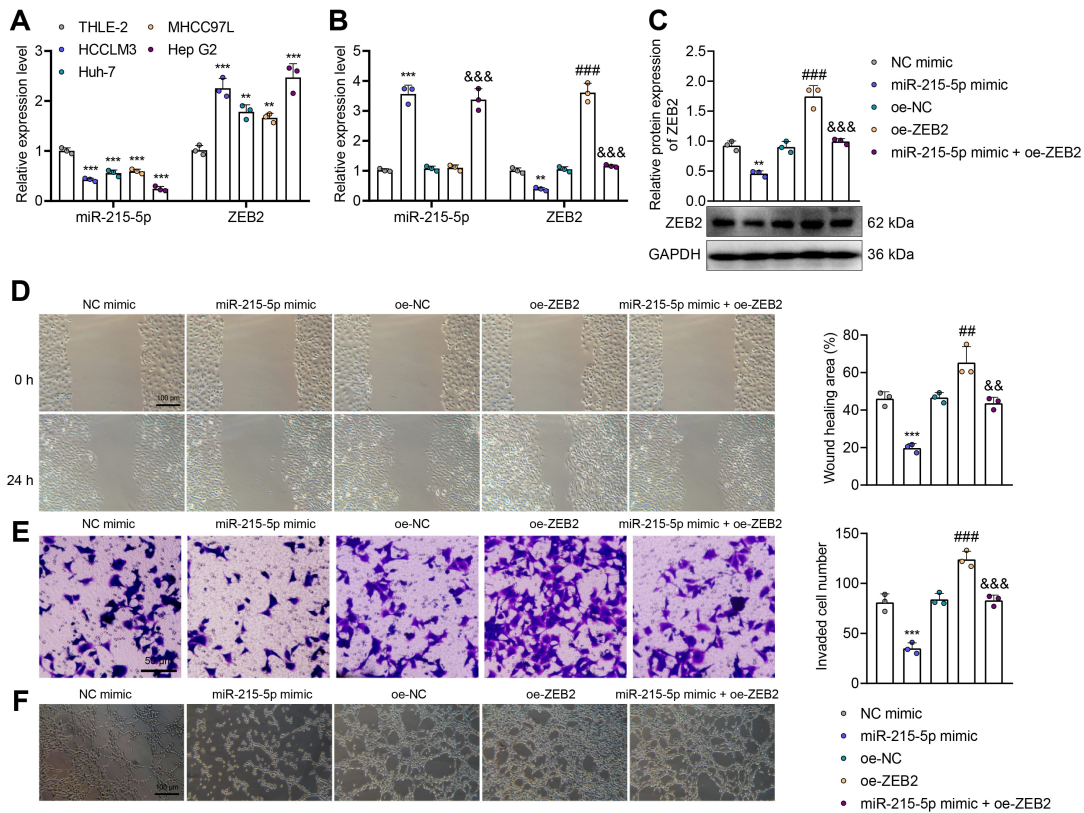


Fig. 7. Effect of miR-215-5p upregulation or *ZEB2* overexpression on invasion, migration, and VM formation abilities by HCC cells *in vitro*. Note: (A) RT-qPCR was used to detect the expression of miR-215-5p and *ZEB2* in human HCC cell lines (HCCLM3, Huh-7, MHCC97L, Hep G2) and human normal liver cell lines (THLE-2). (B) RT-qPCR was used to detect the mRNA expression levels of miR-215-5p and *ZEB2* in each group of cells. (C) Western blot was used to detect the level of *ZEB2* protein expression in cells in each group. (D) The cell migration ability of each group was detected by scratch test. (E) Transwell invasion test was used to detect the invasion ability of cells in each group. (F) In the *in vitro* vascular simulation test, the tubular structure diagram of each group was obtained after 48 hours and 7 days of 3D culturing. The experiment was repeated three times. Compared with the Negative Control (NC) mimic group, ** indicates $p < 0.01$, and *** indicates $p < 0.001$. Compared with the oe-NC group, # indicates $p < 0.01$, and ### indicates $p < 0.001$. Compared with the oe-*ZEB2* group, && indicates $p < 0.01$, and &&& indicates $p < 0.001$.

significant in multiple cancers, promotes HCC cell proliferation, invasion, and metastasis by repressing genes such as *CYLD* and is involved in regulating HCC stem cells and mechanisms, including immune escape and drug resistance [50,51].

Kaplan–Meier curve analysis indicated that high expression of hsa-miR-215-5p is associated with better overall survival in HCC patients compared to low expression, whereas the other seven miRNAs showed no significant impact on survival [13–15,18]. miR-215-5p is related to the invasion, metastasis, and prognosis of HCC, suggesting its potential as a prognostic and therapeutic target [17–19,52].

Further analysis revealed miR-215-5p downregulation in HCC tissues, especially in those with vascular invasion, highlighting its crucial role in HCC malignancy and vascular invasion. This pattern was also observed in other cancers, including gastric and colorectal [53,54]. Subsequent bioinformatics and dual luciferase reporter assays confirmed the target inhibition of *ZEB2* by miR-215-5p and

its association with VM in HCC. This implies that miR-215-5p could prevent HCC vascular invasion and metastasis by inhibiting EMT and VM formation through suppressing *ZEB2*, a pathway also implicated in other malignancies, such as pancreatic and renal cancers [55,56].

Clinical tissue experiments showed low miR-215-5p and high *ZEB2* expression in HCC patients, with a negative correlation of miR-215-5p with VM positivity and recurrent metastasis rate. This suggests that miR-215-5p can reduce HCC recurrent metastasis by targeting *ZEB2*, affecting the VM and angiogenic capacities of HCC cells [18,54,57].

In vitro assays corroborated these findings, showing that miR-215-5p overexpression inhibited *ZEB2*, impacting HCC cell invasion, migration, and VM formation. This indicates the potential of miR-215-5p-targeted *ZEB2* inhibition in reducing HCC angiogenesis and metastasis, a phenomenon also observed in breast and cervical cancers [58,59].

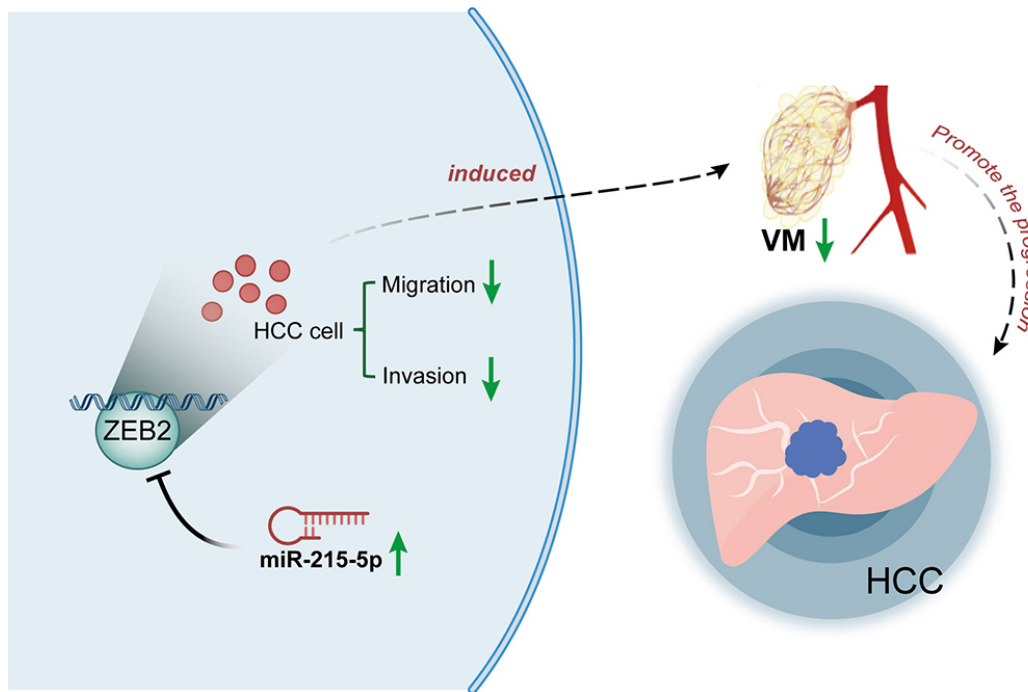


Fig. 8. miR-215-5p prevents vascular invasion and recurrent metastasis of HCC by inhibiting VM.

A study highlighted a decrease in miR-215-5p expression in tumor tissues, with a further reduction in metastatic lesions [56]. In contrast, *ZEB2* overexpression in surrounding liver tissue correlated with favorable survival post-HCC resection [60]. This study also explored the role of VM in HCC, particularly in the context of miR-215-5p and *ZEB2* overexpression [61].

Our study offers new insights into the role of miR-215-5p in HCC vascular invasion and prognosis, suggesting its potential in therapeutic strategies and early diagnosis. However, limitations include the small, single-center sample size and the observational nature of the study, necessitating further research to establish causality.

5. Conclusions

In conclusion, our study suggests a significant inverse relationship between miR-215-5p expression and VM in HCC tissues, while *ZEB2* expression shows a positive correlation with VM. It appears that miR-215-5p could potentially suppress VM in HCC by targeting and downregulating *ZEB2*, which may subsequently inhibit vascular invasion and recurrent metastasis in HCC (Fig. 8).

Availability of Data and Materials

The data that supports the findings of this study are available on request from the corresponding author.

Author Contributions

HZ, XL and LqC wrote the paper and conceived and designed the experiments; XfG, FG and DY analyzed the

data; JIZ, JhZ and QwT collected and provided the sample for this study. All authors have read and approved the final submitted manuscript. All authors have participated sufficiently in the work to take public responsibility for appropriate portions of the content and agreed to be accountable for all aspects of the work in ensuring that questions related to its accuracy or integrity. All authors contributed to editorial changes in the manuscript.

Ethics Approval and Consent to Participate

All participants provided written informed consent, and the study protocol was approved by the Ethics Committee of Shenzhen Hospital, Southern Medical University (SZYYEC-2023-K056).

Acknowledgment

Not applicable.

Funding

This study was supported by Shenzhen Baoan District Science and Technology Plan Basic Research Project (20210505225917001).

Conflict of Interest

The authors declare no conflict of interest.

Supplementary Material

Supplementary material associated with this article can be found, in the online version, at <https://doi.org/10.31083/j.fbe1601006>.

References

- [1] Luo X, Zhang B, Dong S, Zhang B, Chen X. Hepatocellular Carcinoma With Tumor Thrombus Occupying the Right Atrium and Portal Vein: A Case Report and Literature Review. *Medicine*. 2015; 94: e1049.
- [2] Liu R, Yang K, Meng C, Zhang Z, Xu Y. Vasculogenic mimicry is a marker of poor prognosis in prostate cancer. *Cancer Biology & Therapy*. 2012; 13: 527–533.
- [3] Zheng N, Zhang S, Wu W, Zhang N, Wang J. Regulatory mechanisms and therapeutic targeting of vasculogenic mimicry in hepatocellular carcinoma. *Pharmacological Research*. 2021; 166: 105507.
- [4] She Q, Hu S, Pu X, Guo Q, Mou C, Yang C. The effect of hepatocellular carcinoma-associated fibroblasts on hepatoma vasculogenic mimicry. *American Journal of Cancer Research*. 2020; 10: 4198–4210.
- [5] Saw PE, Xu X, Chen J, Song EW. Non-coding RNAs: the new central dogma of cancer biology. *Science China. Life Sciences*. 2021; 64: 22–50.
- [6] Vychytilova-Faltejskova P, Slaby O. MicroRNA-215: From biology to theranostic applications. *Molecular Aspects of Medicine*. 2019; 70: 72–89.
- [7] Sun B, Xing K, Qi C, Yan K, Xu Y. Down-regulation of miR-215 attenuates lipopolysaccharide-induced inflammatory injury in CCD-18co cells by targeting GDF11 through the TLR4/NF-kB and JNK/p38 signaling pathways. *Histology and Histopathology*. 2020; 35: 1473–1481.
- [8] Chen Y, Sun Y, Luo Z, Lin J, Qi B, Kang X, *et al.* Potential Mechanism Underlying Exercise Upregulated Circulating Blood Exosome miR-215-5p to Prevent Necroptosis of Neuronal Cells and a Model for Early Diagnosis of Alzheimer's Disease. *Frontiers in Aging Neuroscience*. 2022; 14: 860364.
- [9] Yin Z, Shen J, Wang Q, Wen L, Qu W, Zhang Y. miR-215-5p regulates osteoporosis development and osteogenic differentiation by targeting XIAP. *BMC Musculoskeletal Disorders*. 2022; 23: 789.
- [10] Xiong X, He Q, Liu J, Dai R, Zhang H, Cao Z, *et al.* MicroRNA miR-215-5p Regulates Doxorubicin-induced Cardiomyocyte Injury by Targeting ZEB2. *Journal of Cardiovascular Pharmacology*. 2021; 78: 622–629.
- [11] Pareek S, Sanchenkova X, Sakaguchi T, Murakami M, Okumura R, Kayama H, *et al.* Epithelial miR-215 negatively modulates Th17-dominant inflammation by inhibiting CXCL12 production in the small intestine. *Genes to Cells: Devoted to Molecular & Cellular Mechanisms*. 2022; 27: 243–253.
- [12] Huang J, Cao Y, Li X, Yu F, Han X. E2F1 regulates miR-215-5p to aggravate paraquat-induced pulmonary fibrosis via repressing BMPR2 expression. *Toxicology Research*. 2022; 11: 940–950.
- [13] Kong X, Duan Y, Sang Y, Li Y, Zhang H, Liang Y, *et al.* LncRNA-CDC6 promotes breast cancer progression and function as ceRNA to target CDC6 by sponging microRNA-215. *Journal of Cellular Physiology*. 2019; 234: 9105–9117.
- [14] Chen JY, Xu LF, Hu HL, Wen YQ, Chen D, Liu WH. MiRNA-215-5p alleviates the metastasis of prostate cancer by targeting PGK1. *European Review for Medical and Pharmacological Sciences*. 2020; 24: 639–646.
- [15] Yan J, Wei R, Li H, Dou Y, Wang J. miR-452-5p and miR-215-5p expression levels in colorectal cancer tissues and their relationship with clinicopathological features. *Oncology Letters*. 2020; 20: 2955–2961.
- [16] Song Z, Bai J, Jiang R, Wu J, Yang W. MicroRNA-215-5p promotes proliferation, invasion, and inhibits apoptosis in liposarcoma cells by targeting MDM2. *Cancer Medicine*. 2023; 12: 13455–13470.
- [17] El Mahdy HA, Abdelhamid IA, Amen AI, Abdelsameea E, Hasouna MM. MicroRNA-215 as a Diagnostic Marker in Egyptian Patients with Hepatocellular Carcinoma. *Asian Pacific Journal of Cancer Prevention: APJCP*. 2019; 20: 2723–2731.
- [18] Xu H, Huang J, Hua S, Liang L, He X, Zhan M, *et al.* Interactome analysis of gene expression profiles identifies CDC6 as a potential therapeutic target modified by miR-215-5p in hepatocellular carcinoma. *International Journal of Medical Sciences*. 2020; 17: 2926–2940.
- [19] Abdelkhalek ZS, Abdalla MS, Fathy MM, Elbaz TM, Abdelaziz AO, Nabeel MM, *et al.* Role of circulating microRNA-21 and microRNA-215 in the diagnosis of hepatitis C related hepatocellular carcinoma. *Journal of Infection in Developing Countries*. 2021; 15: 997–1003.
- [20] Fardi M, Alivand M, Baradaran B, Farshdousti Hagh M, Solali S. The crucial role of ZEB2: From development to epithelial-to-mesenchymal transition and cancer complexity. *Journal of Cellular Physiology*. 2019; 234: 14783–14799.
- [21] Yang S, Li X, Shen W, Hu H, Li C, Han G. MicroRNA-140 Represses Esophageal Cancer Progression via Targeting ZEB2 to Regulate Wnt/ β -Catenin Pathway. *The Journal of Surgical Research*. 2021; 257: 267–277.
- [22] Yu X, Wang W, Lin X, Zheng X, Yang A. Roles of ZEB2 and RBM38 in liver cancer stem cell proliferation. *Journal of B.U.ON.: Official Journal of the Balkan Union of Oncology*. 2020; 25: 1390–1394.
- [23] Burks HE, Matossian MD, Rhodes LV, Phamduy T, Elliott S, Buechlein A, *et al.* ZEB2 regulates endocrine therapy sensitivity and metastasis in luminal a breast cancer cells through a non-canonical mechanism. *Breast Cancer Research and Treatment*. 2021; 189: 25–37.
- [24] Lv J, Zhu S, Chen H, Xu Y, Su Q, Yu G, *et al.* Paeonol inhibits human lung cancer cell viability and metastasis *in vitro* via miR-126-5p/ZEB2 axis. *Drug Development Research*. 2022; 83: 432–446.
- [25] Du Y, Liu X, Zhang S, Chen S, Guan X, Li Q, *et al.* CircCRIM1 promotes ovarian cancer progression by working as ceRNAs of CRIM1 and targeting miR-383-5p/ZEB2 axis. *Reproductive Biology and Endocrinology: RB&E*. 2021; 19: 176.
- [26] Tu J, Ma L, Zhang M, Zhang J. Long Non-Coding RNA SOX2 Overlapping Transcript Aggravates H9c2 Cell Injury via the miR-215-5p/ZEB2 Axis and Promotes Ischemic Heart Failure in a Rat Model. *The Tohoku Journal of Experimental Medicine*. 2021; 254: 221–231.
- [27] Jin J, Wang Y, Zhao L, Zou W, Tan M, He Q. Exosomal miRNA-215-5p Derived from Adipose-Derived Stem Cells Attenuates Epithelial-Mesenchymal Transition of Podocytes by Inhibiting ZEB2. *BioMed Research International*. 2020; 2020: 2685305.
- [28] Korean Liver Cancer Study Group (KLCSG), National Cancer Center, Korea (NCC). 2014 Korean Liver Cancer Study Group-National Cancer Center Korea practice guideline for the management of hepatocellular carcinoma. *Korean Journal of Radiology*. 2015; 16: 465–522.
- [29] Wang D, Ruan X, Liu X, Xue Y, Shao L, Yang C, *et al.* SUMOylation of PUM2 promotes the vasculogenic mimicry of glioma cells via regulating CEBPD. *Clinical and Translational Medicine*. 2020; 10: e168.
- [30] Feng Y, Wang B, Liang G, Wen S, Sun R. Relationship between vasculogenic mimicry and clinic pathological features in laryngeal carcinoma. *Journal of Clinical Otorhinolaryngology, Head, and Neck Surgery*. 2015; 29: 2071–2075. (In Chinese)
- [31] Jin L, Li Y, He T, Hu J, Liu J, Chen M, *et al.* miR 15a 5p acts as an oncogene in renal cell carcinoma. *Molecular Medicine Reports*. 2017; 15: 1379–1386.
- [32] Jiang M, Xu B, Li X, Shang Y, Chu Y, Wang W, *et al.* O-GlcNAcylation promotes colorectal cancer metastasis via the miR-101-O-GlcNAc/EZH2 regulatory feedback circuit. *Oncogene*. 2019; 38: 301–316.

- [33] Ma HL, Yu SJ, Chen J, Ding XF, Chen G, Liang Y, *et al.* CA8 promotes RCC proliferation and migration though its expression level is lower in tumor compared to adjacent normal tissue. *Biomedicine & Pharmacotherapy*. 2020; 121: 109578.
- [34] Sun T, Sun BC, Zhao XL, Zhao N, Dong XY, Che N, *et al.* Promotion of tumor cell metastasis and vasculogenic mimicry by way of transcription coactivation by Bcl-2 and Twist1: a study of hepatocellular carcinoma. *Hepatology (Baltimore, Md.)*. 2011; 54: 1690–1706.
- [35] Yang Z, Sun B, Li Y, Zhao X, Zhao X, Gu Q, *et al.* ZEB2 promotes vasculogenic mimicry by TGF- β 1 induced epithelial-to-mesenchymal transition in hepatocellular carcinoma. *Experimental and Molecular Pathology*. 2015; 98: 352–359.
- [36] Wang Y, Shi F, Tao R, Wu J, Gu J, Yang R, *et al.* The Relationship Between UBE2C and AGGF1 Overexpression and Tumor Angiogenesis in Non-Small Cell Lung Cancer. *Cancer Management and Research*. 2021; 13: 5919–5930.
- [37] Zhang Y, Sun B, Zhao X, Liu Z, Wang X, Yao X, *et al.* Clinical significances and prognostic value of cancer stem-like cells markers and vasculogenic mimicry in renal cell carcinoma. *Journal of Surgical Oncology*. 2013; 108: 414–419.
- [38] Liang C, Yang L, Guo SW, Li RC. Downregulation of Astrocyte Elevated Gene-1 Expression Combined with All-Trans Retinoic Acid Inhibits Development of Vasculogenic Mimicry and Angiogenesis in Glioma. *Current Medical Science*. 2022; 42: 397–406.
- [39] Hendrix MJC, SefTOR EA, Hess AR, SefTOR REB. Molecular plasticity of human melanoma cells. *Oncogene*. 2003; 22: 3070–3075.
- [40] Hendrix MJC, SefTOR EA, Hess AR, SefTOR REB. Vasculogenic mimicry and tumour-cell plasticity: lessons from melanoma. *Nature Reviews. Cancer*. 2003; 3: 411–421.
- [41] Thapa N, Chwae YJ, Yoo KH, Won TB, Kang D, Choi D, *et al.* Exosomal delivery of TRAIL and miR 335 for the treatment of hepatocellular carcinoma (Review). *International Journal of Molecular Medicine*. 2023; 51: 3.
- [42] Yuan J, Ji H, Xiao F, Lin Z, Zhao X, Wang Z, *et al.* MicroRNA-340 inhibits the proliferation and invasion of hepatocellular carcinoma cells by targeting JAK1. *Biochemical and Biophysical Research Communications*. 2017; 483: 578–584.
- [43] Xie L, Chen Z, Liu H, Guan L, Wang Z, Li W. Effects of miR-340 on hepatocellular carcinoma by targeting the DcR3 gene. *Digestive and Liver Disease: Official Journal of the Italian Society of Gastroenterology and the Italian Association for the Study of the Liver*. 2018; 50: 291–296.
- [44] Zhu XM, Wu LJ, Xu J, Yang R, Wu FS. Let-7c microRNA expression and clinical significance in hepatocellular carcinoma. *The Journal of International Medical Research*. 2011; 39: 2323–2329.
- [45] Chen H, Kong M, Chen Y, Jiang Y, Wen M, Zhang X. Prognostic significance of miR-203 and ZEB1 expression in early-stage hepatocellular carcinoma. *Journal of Cancer*. 2021; 12: 4810–4818.
- [46] Zheng XB, Chen XB, Xu LL, Zhang M, Feng L, Yi PS, *et al.* miR-203 inhibits augmented proliferation and metastasis of hepatocellular carcinoma residual in the promoted regenerating liver. *Cancer Science*. 2017; 108: 338–346.
- [47] Zhu Y, Liu Y, Xiao B, Cai H, Liu M, Ma L, *et al.* The circular RNA PVT1/miR-203/HOXD3 pathway promotes the progression of human hepatocellular carcinoma. *Biology Open*. 2019; 8: bio043687.
- [48] Shi Y, Yang X, Xue X, Sun D, Cai P, Song Q, *et al.* HANR promotes hepatocellular carcinoma progression via miR-214/EZH2/TGF- β axis. *Biochemical and Biophysical Research Communications*. 2018; 506: 189–193.
- [49] Wang Y, Lee CGL. Role of miR-224 in hepatocellular carcinoma: a tool for possible therapeutic intervention? *Epigenomics*. 2011; 3: 235–243.
- [50] Ai J, Gong C, Wu J, Gao J, Liu W, Liao W, *et al.* MicroRNA 181c suppresses growth and metastasis of hepatocellular carcinoma by modulating NCAPG. *Cancer Management and Research*. 2019; 11: 3455–3467.
- [51] Abd ElAziz ON, Elfiky AM, Yassin MA, Abd El-Hakam FEZ, Saleh EM, El-Hefnawi M, *et al.* *In Silico* and *In Vivo* Evaluation of microRNA-181c-5p's Role in Hepatocellular Carcinoma. *Genes*. 2022; 13: 2343.
- [52] Cho HJ, Eun JW, Baek GO, Seo CW, Ahn HR, Kim SS, *et al.* Serum Exosomal MicroRNA, miR-10b-5p, as a Potential Diagnostic Biomarker for Early-Stage Hepatocellular Carcinoma. *Journal of Clinical Medicine*. 2020; 9: 281.
- [53] Xu YJ, Fan Y. MiR-215/192 participates in gastric cancer progression. *Clinical & Translational Oncology: Official Publication of the Federation of Spanish Oncology Societies and of the National Cancer Institute of Mexico*. 2015; 17: 34–40.
- [54] Chen DL, Lu YX, Zhang JX, Wei XL, Wang F, Zeng ZL, *et al.* Long non-coding RNA UICLM promotes colorectal cancer liver metastasis by acting as a ceRNA for microRNA-215 to regulate ZEB2 expression. *Theranostics*. 2017; 7: 4836–4849.
- [55] Khella HWZ, Bakhet M, Allo G, Jewett MAS, Girgis AH, Latif A, *et al.* miR-192, miR-194 and miR-215: a convergent microRNA network suppressing tumor progression in renal cell carcinoma. *Carcinogenesis*. 2013; 34: 2231–2239.
- [56] Machackova T, Vychytilova-Faltejskova P, Souckova K, Trachtova K, Brchnelova D, Svoboda M, *et al.* MiR-215-5p Reduces Liver Metastasis in an Experimental Model of Colorectal Cancer through Regulation of ECM-Receptor Interactions and Focal Adhesion. *Cancers*. 2020; 12: 3518.
- [57] White NMA, Khella HWZ, Grigull J, Adzovic S, Youssef YM, Honey RJ, *et al.* miRNA profiling in metastatic renal cell carcinoma reveals a tumour-suppressor effect for miR-215. *British Journal of Cancer*. 2011; 105: 1741–1749.
- [58] Wang M, Liao J, Tan C, Zhou H, Wang J, Wang K, *et al.* Integrated study of miR-215 promoting breast cancer cell apoptosis by targeting RAD54B. *Journal of Cellular and Molecular Medicine*. 2021; 25: 3327–3338.
- [59] Liu CQ, Chen Y, Xie BF, Li YL, Wei YT, Wang F. MicroRNA-215-3p suppresses the growth and metastasis of cervical cancer cell via targeting SOX9. *European Review for Medical and Pharmacological Sciences*. 2019; 23: 5628–5639.
- [60] Cai MY, Luo RZ, Chen JW, Pei XQ, Lu JB, Hou JH, *et al.* Overexpression of ZEB2 in peritumoral liver tissue correlates with favorable survival after curative resection of hepatocellular carcinoma. *PLoS One*. 2012; 7: e32838.
- [61] Li X, Sun B, Zhao X, An J, Zhang Y, Gu Q, *et al.* Function of BMP4 in the Formation of Vasculogenic Mimicry in Hepatocellular Carcinoma. *Journal of Cancer*. 2020; 11: 2560–2571.